UNIVERSITY OF TARTU
Faculty of Science and Technology
Institute of Technology

Jürgen-Martin Assafrei

Bismuth Metal-Organic Framework Based Catalyst for CO_2 Electroreduction

Bachelor's Thesis (12 ECTS)

Curriculum Science and Technology

Supervisor:

Assoc. Professor, PhD Nadezda Kongi

Tartu 2021

Bismuth Metal-Organic Framework Based Catalyst for CO_2 Electroreduction

Abstract:

Electrochemical reduction of CO_2 into different fuels and other valuable chemicals is a highly promising method of CO_2 valorisation. Among the many possible compounds that CO_2 can be reduced to, formic acid is especially attractive because it already has quite a large market in agriculture and the pharmaceutical industry. It can be used directly in a formic acid fuel cell or as hydrogen storage for hydrogen fuel cells. The catalysts used for this reduction process need to strongly absorb CO_2 and show poor activity towards the hydrogen evolution reaction (HER) so that it would not interfere. This work focuses on Bi-N-C electrocatalysts fabricated by carbonization of TAL33 MOF compounds at different temperatures. The electrochemical activity of the catalysts was measured, and some samples showed Faradaic efficiencies up to 100 % and formed formic acid at concentrations up to 20 mM after 90 minutes. To investigate why samples at different carbonization temperatures showed different results, surface morphological studies were conducted. Results obtained in electrochemical experiments were further confirmed by theoretical calculations.

Keywords: CO_2 electroreduction; Bismuth; Metal-Organic Framework; Formate; Green Formic Acid.

CERCS: P401 Electrochemistry

Vismuti Metallorgaanilisel Võrestikul Põhinev Katalüsaator CO_2 Elektroredutseerumiseks

Lühikokkuvõte:

Elektrokeemiline CO_2 redutseerimine on muutumas populaarseks teemaks alades nagu, rohelise energia hoiustamine väärtuslike kemikalidena. Kõikidest võimalikes kemikaalidest, milleks saab CO_2 redutseerida, on metaanhape eriti huvitav, sest metaanhappel on suur olemasolev turg põllumajanduses ja meditsiinis. Metaanhapet saab ka kasutada vesiniku kandjana või kasutada otse kütusena metaanhappe kütuseelementides. Katalüsaatorid mida kasutatakse CO_2 redutseerimiseks metaanhappeks peavad siduma tugevalt CO_2 ja olema vähe aktiivsed vesiniku eraldumise reaktsiooni suhtes, mis on konkureeriv kõrvalreaktsioon. Selles töös fokuseeritakse Bi-N-C katalüsaatoritel, mis on valmistatud TAL33 MOF materjali karboniseerimisel erinevatel temperatuuridel. Valmistatud katalüsaatorite elektrokeemilise aktiivsuse mõõtmise käigus näitasid osad proovid Faraday effektiivsust kuni 100 % ja toodetud metaanhappe kontsentratsioon peale 90 minutit oli kuni 20 mM. Selleks et uurida, miks osadel temperatuuridel valmistatud proovid olid aktiivsemad, teostati morfoloogilised uuringud. Elektrokeemiliste mõõtmiste teel saadud tulemused leidsid kinnitust teoreetiliste modelleerimistega.

Võtmesõnad: CO_2 elektrokeemiline redutseerimine, vismut, metallorgaaniline võrestik, roheline metaanhape.

CERCS: P401 Elektrokeemia

Table of Contents

TERMS, ABBREVIATIONS AND NOTATIONS

AgCl/Ag – silver chloride electrode

CO_2RR – CO_2 reduction reaction

CV – cyclic voltammetry

DFT – density functional theory

e^- – electron

FE – Faradaic efficiency

HER – hydrogen evolution reaction

LM – catalyst consisting of a ligand and a metal ion

MOF – metal-organic framework

ppm – parts-per-million

RHE – reversible hydrogen electrode

SEM – scanning electron microscopy

TEM – transmission electron microscopy

XPS – X-ray photoelectron spectroscopy

XRD – X-ray diffraction

INTRODUCTION

Over the past century, human industrial production and development has led to the amount of carbon dioxide (CO_2) produced to be larger than the amount that is consumed. This imbalance has led to issues like holes in the ozone layer and global warming. The concentration of greenhouse gas CO_2 in the atmosphere has passed the 400 ppm mark.[1] Because of that, reducing the amount of CO_2 produced by converting it into something useful is a must, since cutting all polluting production is not a possible option and changing the entire fossil fuel-based infrastructure takes too much time. For this reason, many governments have started to invest in green technologies and attempt with to help along all research that could help solve the impending crisis. There are many possible solutions to the problem and most of them are based on the capture and storage of CO_2. One of the most focused on and researched ways to tackle the problem is electrochemically reducing the CO_2 molecule, where electrical energy is used in an electrochemical system to transform CO_2 into numerous forms. One of the most promising compounds that CO_2 can be reduced to is formic acid, which has multiple uses in medicine, agriculture and the textile industry. Formic acid could also be used for hydrogen storage or direct fuel in formic acid fuel cells [2]. In this work, an efficient electrocatalyst for CO_2 reduction reaction was synthesized from a bismuth-based metal-organic framework (TAL33) (Figure 1). TAL33 was post-synthetically treated and its electrochemical properties were measured by cyclic voltammetry technique. Morphology of the samples was studied using scanning electron microscopy (SEM), transmission electron microscopy (TEM), X-ray diffraction (XRD) and X-ray photoelectron spectroscopy (XPS). Experiments showed that the after optimized post-synthetic carbonization TAL33 MOF is an excellent single-precursor source for Bi-N-C electrocatalyst.

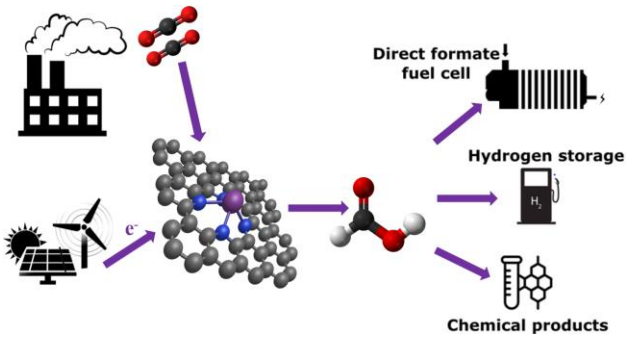

Figure 1. *CO_2 electroreduction to formic acid on Bi-N-C catalyst and potential applications.*

1. LITERATURE REVIEW

1.1 CO_2 electrochemical reduction

The electrochemical reduction of CO_2 is particularly attractive as an option for the storage of excess renewable energy produced by solar panels, wind farms and other forms of green energy production. The energy could be stored as chemical fuels. One of the biggest issues for many renewable energy sources is that instead of constant production of energy, they tend to overproduce or underproduce. To solve this, the fuels would be produced during the overproduction periods and they would be utilized to generate power during the underproduction period, thus solving one of the largest issues of renewable energy sources [3].

CO_2 can be chemically converted into various chemicals, ranging from compounds containing only one carbon atom, like methane (CH_4), up to compounds containing four carbon atoms, like butane (C_4H_{10}) [2,4]. The reduction of CO_2 can proceed through different pathways, which can be two- to eight-electron reductions at different potentials, mediated by different types of electrocatalysts (Figure 2). Some of the major products of this reaction are carbon monoxide (CO), formic acid (HCOOH), methane (CH_4), formate ($HCOO^-$), ethanol (CH_3CH_2OH), methanol (CH_3OH), ethylene (CH_2CH_2) and oxalic acid ($H_2C_2O_4$). There are many challenges in the conversion process, but the potential is great [5].

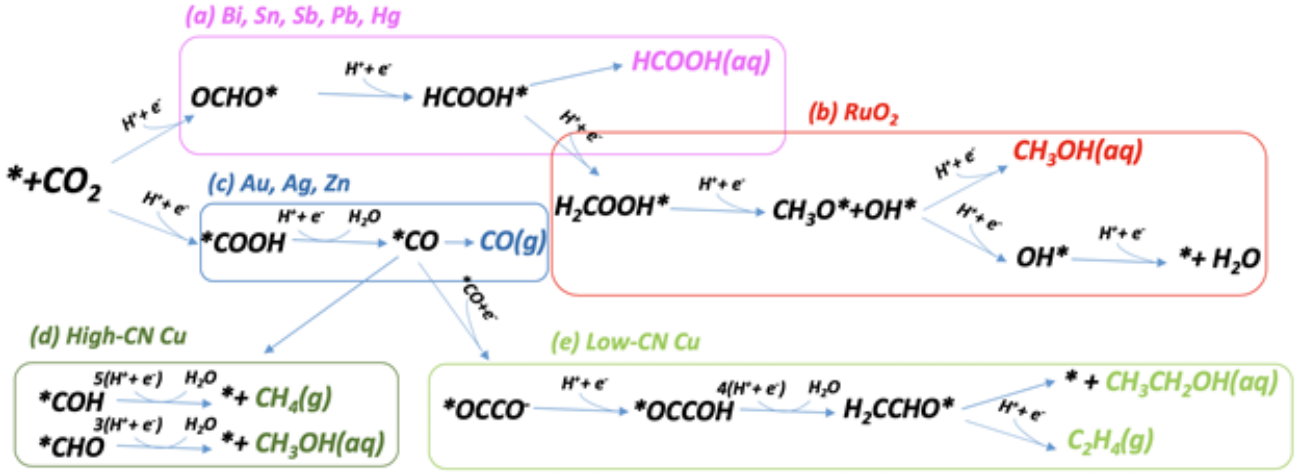

Figure 2. *Possible products and reaction mechanisms of CO_2 electrochemical reduction*

Commonly thought of as the first step in the electrochemical reduction, also as the rate-determining step, is the formation of CO_2^- radical by first e^- transfer. This results in some problems because the standard electrode potential of formation of CO_2^- is -1.9 V vs reversible hydrogen electrode

(RHE). Since the potential of -1.9 V is more negative than the potential needed for hydrogen evolution, then the reduction of CO_2 in an aqueous solution will have strong competition from the hydrogen evolution reaction (HER). Furthermore, because the potentials of formation of compounds like formic acid, methane and methanol are more positive than the potential for the radical CO_2^- formation, then the reaction will be difficult to stop at the desired step for getting the desired product [6]. Such issues can sometimes be overcome by using catalysts that are purposefully made to act as $2e^-$ reservoirs, which will use multiple e^- transfer pathways. Often metal complexes are used to form metallocarboxylate intermediates to produce formate [7].

Typically, the CO_2 reduction reaction is performed in a cell type reactor. The reactor contains a cathode and an anode, the cathode reduces the CO_2 and produces compounds like CO, formic acid and it also produces OH^- ions. The anode oxidizes water during the oxygen evolution reaction, consuming OH^- ions or producing H^+ and electrons. Separating the electrodes is an ion-exchange membrane or a porous diaphragm. The reactor is filled with an electrolyte that dissolves and transports the CO_2. Also, a potential source is needed to transfer electrons between the electrodes [8]. The CO_2 reduction reaction involves several steps. The first step is the mass transfer of gaseous CO_2 into the electrolyte, followed by the transport of CO_2 onto the cathode. Then the CO_2 is absorbed at the surface of the cathode and dissociated into intermediates like *COOH, *CO, *CHO and *COH. Next follows the transport of electrons to the intermediates, then the newly formed products desorb and migrate away from the cathode to the electrolyte [8].

The electrochemical reduction of CO_2 can be performed through a few different mechanisms, either direct or indirect. In the direct mechanism, CO_2 dissolved in the electrolyte or coordinated at the electrode surface receives electrons from the catalysts, which act as electrodes. In the indirect mechanism, the electrons are transported by catalyst molecules, acting as mediators for the electrons to the CO_2 molecule [7].

The positively charged catalyst LM^+ (L-ligand, M-metal ion) gains an electron pair and proton from the solution during the indirect mechanism. This forms a complex LM-H, which reacts with CO_2 to form an LM-CO_2-H intermediate molecule, as shown in Figure 3. Said intermediate then dissociates into LM^+ and CO_2-H, which can either form formic acid or formate, methanol can also be produced, but multiple electron and proton transfers are needed [7].

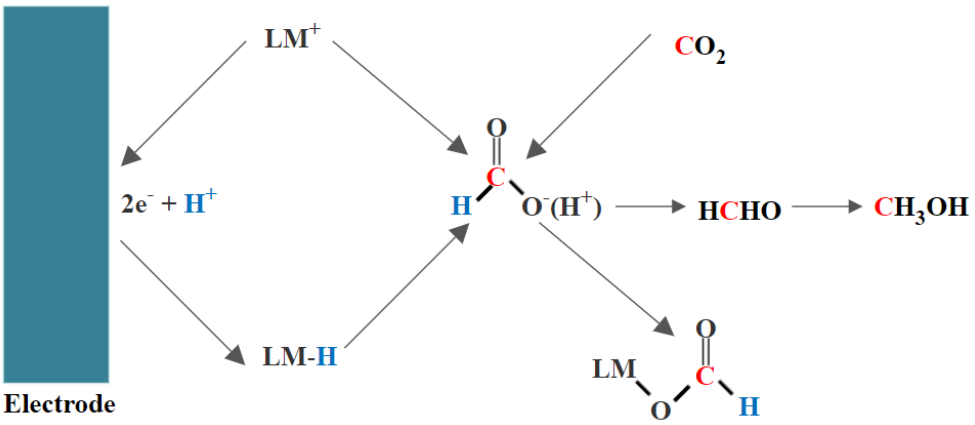

Figure 3. *The indirect mechanism for CO_2 reduction*

Direct mechanisms take place either in the electrolyte solution or directly at the electrode surface. The reaction occurs in the electrolyte when the coordination of electrode surface and CO_2 is not strong enough. The reduction happens during the diffusion of CO_2 to the electrode surface from the solution. The first step, as shown in Figure 4 is the single electron transfer to form the CO_2^- intermediate, after this, there are three different possibilities, two CO_2^- intermediates can form a bond to make $C_2O_4^{2-}$ [9], the CO_2^- intermediate forms an ester bond with a CO_2 molecule, which decomposes into CO and CO_3^{2-} [10] and if the CO_2^- intermediate forms a bond with a proton in the solution, then formate will form [11]. On the other hand, if the coordination between electrode and CO_2 is strong, the CO_2 will coordinate on the electrode surface, as seen in Figure 5. The chemical properties of such electrodes play a large role in the products of the reduction reaction. The CO_2 molecule is coordinated at the electrode surface and during electron transfer, a CO_2^- intermediate is formed. Said intermediate forms a bond with a proton to form COO-H, after another electron is transferred to the COO-H molecule, after which it dissociates into H_2O and CO. However, in some cases, when the catalyst at the electrode surface has a strong interaction with the CO molecule, the CO molecule stays coordinated and is reduced further. The coordinated CO molecule can go through many electron transfers and protonations to form many types of products like aldehydes, alkenes, alkanes and alcohols such as ethane (C_2H_6), methane, ethanol, methanol and others [12]. Another possible option is to have catalysts with dual active sites which respectively bind to CO_2 and hydrogen. The active sites can be arranged so that the formation of C-H bonds would be easier and formate is produced [13].

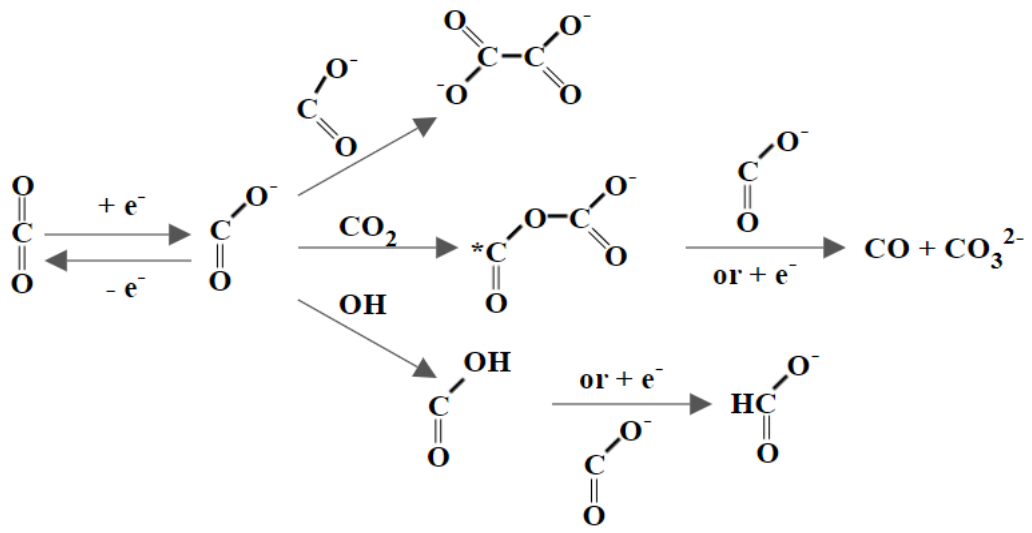

Figure 4. *Direct CO_2RR mechanism in bulk solution*

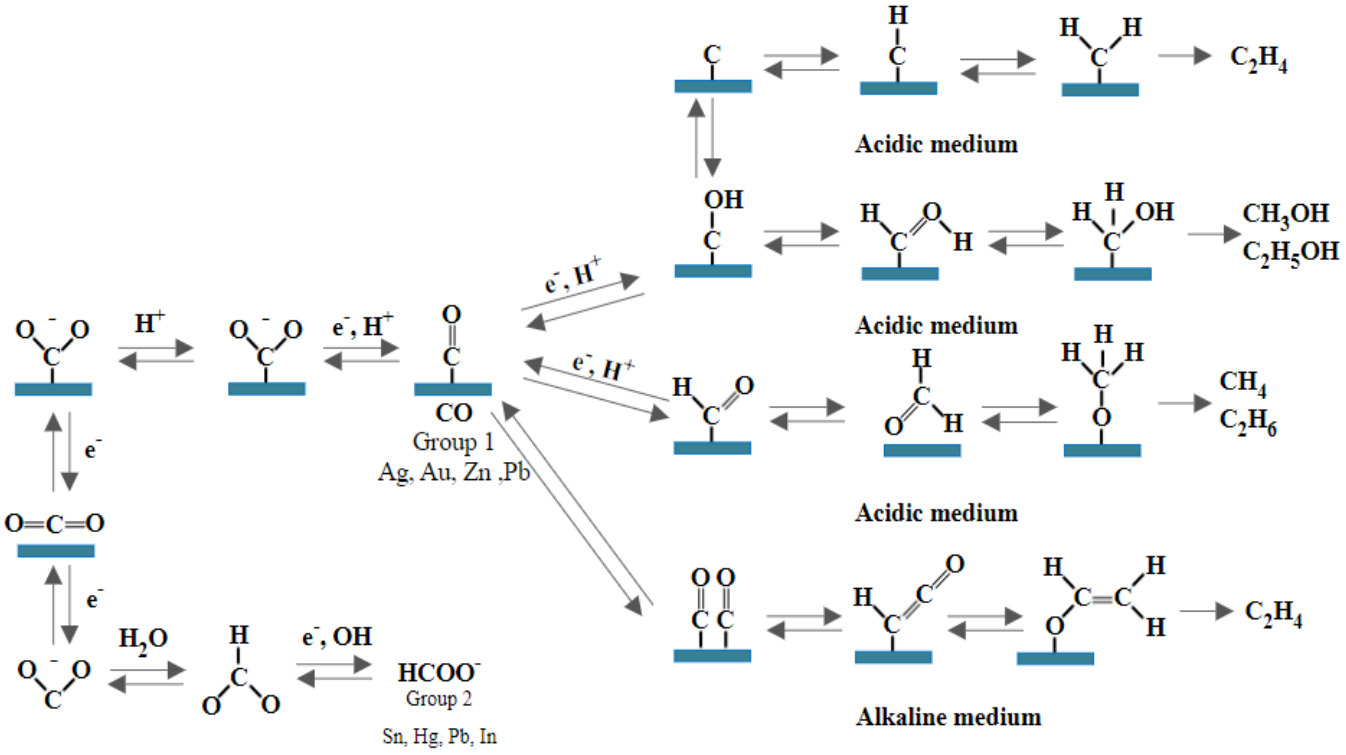

Figure 5. *Direct CO_2RR mechanism at electrode surface*

1.2 CO_2 electroreduction to formate/formic acid

The electrochemical reduction of CO_2 into formic acid or formate, depending on pH, is a very promising strategy in fighting climate change while storing energy in a stable compound [14]. Out of all the possible compounds, which could be synthesized from CO_2, formic acid is promising because of its wide applications. Formic acid has a relatively high hydrogen density of 52 g of H_2 per litre, which makes it a good material for hydrogen storage [15]. It can also be utilized in formic acid fuel cells directly without any preliminary treatment [16]. Annually roughly 950 thousand tons of formic acid is produced and the market for it is growing. Most of the currently used formic acid is produced by the hydrolysis of methyl formate, which heavily depends on the usage of fossil fuels [17].

Formic acid is used in agriculture, the textile industry and the pharmaceutical industry, where it is used to make antiseptics. Because of recent developments around the world, the demand for antiseptics has grown and so has the size of the market for formic acid. The global formic acid market was worth 756.4 million USD back in 2018 and it is anticipated to rise to 828.1 million USD by 2025. [18]

The reduction of CO_2 into formic acid can follow many different pathways depending on the characteristics of the catalyst. Some probable pathways are: CO_2 insertion, C-bound intermediate, O-bound intermediate and bicarbonate intermediate [16]. In the CO_2 insertion pathway, the CO_2 forms a bond with hydrogen from a metal-H bond, which forms an *HCOO intermediate that is then further reduced into formic acid (see Figure 6). This mechanism occurs mainly on lead-based catalysts because of their strong hydrogen binding affinity [19].

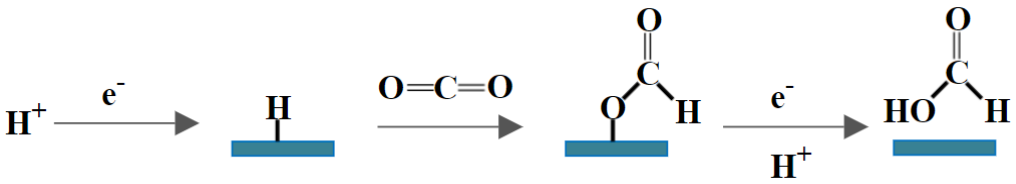

Figure 6. *CO_2 reduction through CO_2 insertion*

In the pathway that uses a C-bound intermediate, shown in Figure 7, first the CO_2^- radical is formed by single-electron transfer, bound to the catalyst by the carbon atom. The intermediate reacts with an H^+ to form *COOH, which is then converted into formic acid. Since the *COOH intermediate is unstable and tends to decompose, then metal catalysts stabilize it into a much more stable

intermediate of *HCOO to then produce formate or formic acid. Mainly catalysts based on copper or ruthenium are used to produce formic acid through such a pathway [20].

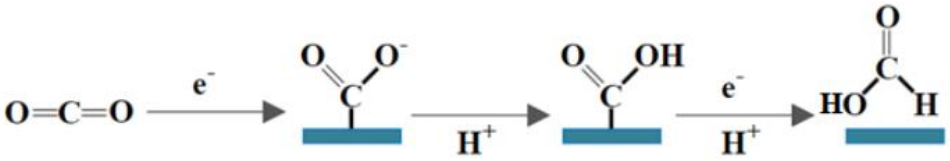

Figure 7. *CO_2 reduction through C-bound intermediate*

The pathway that continues through an O-bound intermediate starts similarly with the formation of the CO_2^- radical, which is weakly bound to the catalyst by the oxygen atoms. The bound CO_2^- radical then reacts with an electron and hydrogen to form formate, which can be further reduced into formic acid. Some of the catalysts that follow this pathway are based on metals like lead, indium, bismuth, lead and mercury, because of the easier formation of HCOO* over the COOH* intermediate, as shown in Figure 8 [16].

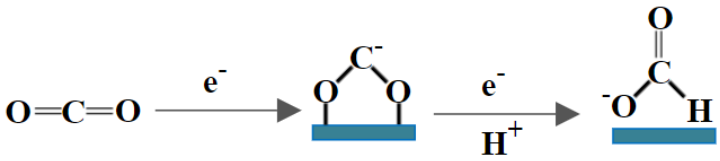

Figure 8. *CO_2 reduction through O-bound intermediate*

The bicarbonate intermediate based pathway begins by CO_2 reaction with the OH, which is adsorbed on the catalyst surface. The reaction produces CO_3H* intermediate, which is adsorbed, the CO_3H* intermediate reacts with an electron and a hydrogen ion, forming HCOO*, which reacts with another hydrogen ion and another electron to form HCOOH and leave behind a catalyst bound OH group. Such a reaction pathway has been observed on catalysts like $PdSnO_2$, SnO_x and on Bi-Sn interfaces. Most likely, this pathway occurs on catalysts that bind OH groups relatively strongly, as shown in Figure 9 [21].

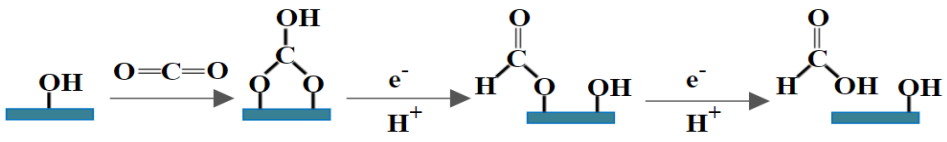

Figure 9. *CO_2 reduction through bicarbonate intermediate*

1.3 Bismuth-based electrocatalysts

On the one hand, there are many environmentally unfriendly or way too expensive catalysts that exhibit a production preference of formic acid, such as noble metals like platinum, heavy metals like mercury, lead, thallium and cadmium. Bismuth composites, on the other hand, exhibit high activity and selectivity towards formic acid. This is because bismuth compounds have strong adsorption of the CO_2^- intermediate. Moreover, it shows poor activity for hydrogen evolution reaction. Meaning that the HER reaction does not interfere with the CO_2 reduction reaction (CO_2RR) [22].

Because of this, bismuth has recently started to gain popularity as a promising electrocatalytic material for the production of formic acid, *via* electrocatalytic reduction of CO_2, with an increasing number of studies published on the matter early [2]. In recent studies, the electrode configurations used for the electrochemical conversion of CO_2 to formic acid have varied quite significantly. Examples of these are electrodes based on bismuth particles synthesized on copper and titanium substrate [23], bismuth particles synthesized onto copper surface [24], oxide-derived bismuth films [25], carbon-supported bismuth nanoparticles [26] and bismuth nanosheets [27]. Zhong *et al.* used nanostructured bismuth dendrite electrocatalyst, which was grown on carbon paper, to show good performance in CO_2RR into formic acid. The maximum achieved faradaic efficiency was 96.4% and current density of 15.2 mA cm^{-2} at 1.8V [28]. In another study by Zhang *et al.* BiOCl nanosheets were used under ambient pressure and temperature in the electrochemical reduction of CO_2 into formic acid and the produced faradaic efficiency was 92% and current density of 3.7 mA mg^{-1} at -1.5V [29]. All of the studies mentioned above were carried out in an aqueous bicarbonate medium. Recent studies show very promising results and because of this, the attention to study the electrochemical valorisation of CO_2 to obtain formate using a bismuth-based catalyst is growing rapidly.

Metal-organic framework materials are highly crystalline and porous hybrid materials made by linking metal clusters and organic ligands *via* coordinate bonds [30]. Because of their high porosity and large surface specific area, which are highly beneficial for charge transfer, MOF derived materials have been applied as promising catalyst materials for the electrochemical reduction of CO_2 [31]. In previous studies, many different MOF catalysts have proven to be good catalysts for CO_2RR. But their uses are limited because of charge transfer characteristics and selectivity. Also,

the structural stability of MOF materials is a concern. To solve this, carbonization and electrochemical transformation processes are used to enhance the stability or activity of the MOF (Figure 10) [32]. Therefore, accounting for the great performance of bismuth-based materials in CO_2RR and the excellent results of MOFs and the catalysts made from them, it makes sense to use Bi-MOF materials as catalysts to produce formic acid out of CO_2 [33].

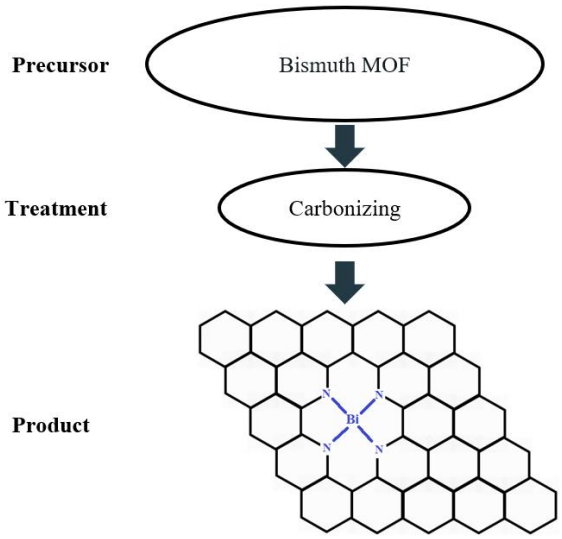

Figure 10. *Fabrication of Bi-N-C materials*

2. AIMS OF THE THESIS

The main aims of this thesis are:

- Aim 1. To synthesise Bi-N-C electrocatalytic material.
- Aim 2. To establish an optimized post-synthetic treatment of the electrocatalytic material.
- Aim 3. To conduct morphological studies of the electrocatalytic material.
- Aim 4. To electrochemically screen the electrocatalytic material.
- Aim 5. To compare the electrocatalytic activity of TAL33-based catalysts carbonized at different temperatures.
- Aim 6. To understand the catalytic mechanism by morphology vs electrochemical response results.

3. EXPERIMENTAL PART

3.1 METHODS

3.1.1 Synthesis and carbonization

TAL33 MOF material was synthesized using 1H-benzo[d]imidazole-5,6-diol linker and Bi-metal precursor ($BiCl_3$). Synthesis of 1H-benzo[d]imidazole-5,6-diol was performed using an earlier published procedure [[34]]. $BiCl_3$ (3.15 g, 9.99 mmol, 1.0 equiv) was slowly added into a mixture of 1H-benzo[d]imidazole-5,6-diol (3.00 g, 19.98 mmol, 2.0 equiv) in 25% aq. NH_3/DMF/EtOH/water (4:10:10:15), the resulting solution was left to stir at room temperature. After 24 h, it was filtered, washed with EtOH and dried to give the desired material (4.98 g).

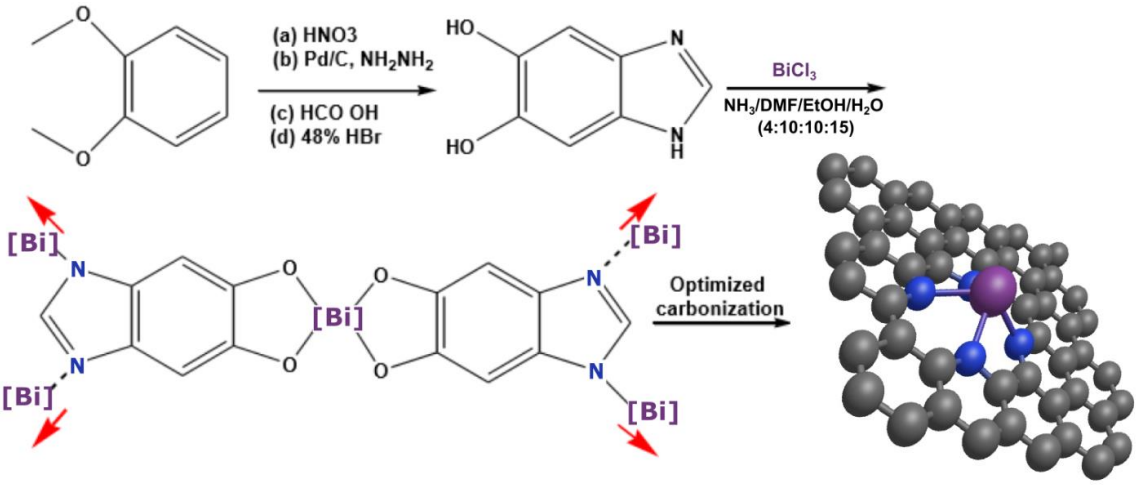

Figure 11. *Synthesis of Bi-N-C material*

A series of Bi-N-C materials were prepared by carbonizing the TAL33 MOF at 300 °C and up to 700 °C with an interval of 100 °C in a tube furnace, leading to 5 samples being made: Bi300, Bi400, Bi500, Bi600 and Bi700. Carbonization of the material was done following a rapid heating process in an inert gas (N_2) atmosphere. The material is placed into a ceramic boat, which was moved into the furnace tube after the specified temperature was reached. The temperature was kept constant for 2 hours. After the heating, the heater was turned off and the material was left to cool down naturally. After carbonization, obtained Bi-N-C samples were designated as Bi300, Bi400, Bi500, Bi600 and Bi700. The morphology of prepared catalysts was examined by SEM, TEM, XPS and XRD. The electrochemical behaviour of new catalyst materials was investigated by cyclic voltammetry technique.

3.1.2 Morphology measurements

Powder X-ray diffraction (PXRD) measurements were performed on a Bruker D8 Advance instrument. The ICDD PDF-4 + database (2020) was used for qualitative analysis. Bruker Topas 6 software was used for full profile analysis.

The surface morphology of the material was examined using a scanning electron microscopy (SEM) with FEI HR-SEM NanoSem 450. SEM samples were prepared by drop-coating a catalyst suspension onto polished GC plates.

The X-ray photoelectron spectroscopy (XPS) experiments were conducted at ultra-high vacuum conditions with a non-monochromatic twin anode X-ray tube (Thermo XR3E2) which has the characteristic energy of 1253.6 eV (Mg K_{α}). Electron energy analyzer was SCIENTA SES 100. The data was processed by CasaXPS software (version 2.3.17).
The TEM images were taken using a JEM-2010 microscope (JEOL, Akishima) at 200 kV with a JEOL JEM-1400 Plus working at 120 kV. The measured samples were dispersed onto a Formvar-covered copper grid and evaporated in air at room temperature.

3.1.3 Electrochemical measurements, electrode preparation and setup

The catalytic ink, for application of catalyst onto the electrode surface, was made by dispersing the sample in a Nafion solution (perfluorosulfonic acid- PTFE copolymer 5 % w/w solution, Alfa Aesar) at Bi-N-C: Nafion mass ration of 80:20. The mixture was diluted 50-fold to 2 % in absolute ethanol (EMSURE). An ultrasonic bath was used for homogenization the ink for roughly 30 minutes. The cathode was prepared by air-brushing the ink on a 6 cm^2 Toray paper (TGPH-120, QuinTech), on a heated metallic plate at 90°C for faster evaporation. The bismuth loading was 1 mg/cm^2.

The electrochemical activity of Bi-N-C material was performed in a standard three-electrode configuration glass cell in 0.45M $KHCO_3$ (99.7 % Sigma Aldrich) and 0.5 M KCl (99.5 %, Emsure) solution, saturated by CO_2 or Ar, using an AgCl/Ag (3.5M KCl) as the reference electrode and a Pt wire as the counter electrode. Cyclic voltammetry was performed using PGSTAT302N (Metrohm Autolab B. V.). All cyclic voltammetry measurements were performed at room temperature (25 °C) and the currents were normalized by the geometric area of the electrodes. CO_2RR was performed in an H-type cell that has compartments that are divided by a cationic

exchange membrane (Nafion 112). A 0.45M $KHCO_3$ and 0.5 M KCl solution saturated with CO_2 was used as catholyte. 1.0 M KOH (85% Panreac) solution was used as anolyte. The cation exchange membrane was activated in 0.1 M NaOH solution for 24 hours. A nickel mesh immersed in the anolyte was used as a counter electrode and AgCl/Ag placed in the catholyte as a reference electrode. The CO_2RR was carried out by chronoamperometry measurements at a controlled potential of -1.7 V for 1.5 hours using the same PGSTAT302N. The reduction of CO_2 into formic acid was followed by ionic chromatography (883 Basic IC plus, Metrohm), with a conductivity range of 15000 μScm−1. The mobile phase consisted of 1.8 mM Na_2CO_3 and 1.7 Mm $NaHCO_3$ solution. The calibration curve was carried out from 0 to 30 ppm in solution of 0.0045 M $KHCO_3$ and 0.005 M KCl (corresponding with a 100 times dilution of the catholyte).

3.2 RESULTS AND DISCUSSION

3.2.1 Electrochemical characterization

The electrochemical reduction electrolysis was performed in an H-type cell to evaluate the product formed, FE and selectivity towards formic acid. For all four samples, the electrolysis was performed at -1.7 V for 90 minutes in a CO_2 saturated 0.45 M KHCO3 and 0.5 M KCl solution. Cyclic voltammetry (CV) was performed in Ar/CO2-saturated 0.45 M KHCO3 and 0.5 M KCl solution. Main kinetic parameters were obtained from CV data, such as CO_2RR onset potential and FE. The obtained results show a well-defined CO_2 reduction process starting at about -1.4 V vs AgCl/Ag.

Faradaic efficiency is an important parameter for understanding the selectivity towards a certain product in a CO_2RR. It describes the efficiency of charge transfer in an electrochemical reaction. The FE can be calculated by dividing the charge consumed to produce a certain amount of product (formic acid) by the total charge passed through the cathode. FE can be calculated using following eq.:

$$FE = nNF/Q \quad (1)$$

where n stands for the mole of e^- needed to produce one mole of formic acid (n = 2), N stands for the mole of formic acid identified, F stands for the Faradaic constant (96 485 C mol^{-1}) and Q stands for the charge consumed at the cathode during the reaction.

Cyclic voltammetry measurements were conducted with samples Bi300 – Bi700 and the cyclic voltammograms of sample Bi400 can be seen in Figure 12a.

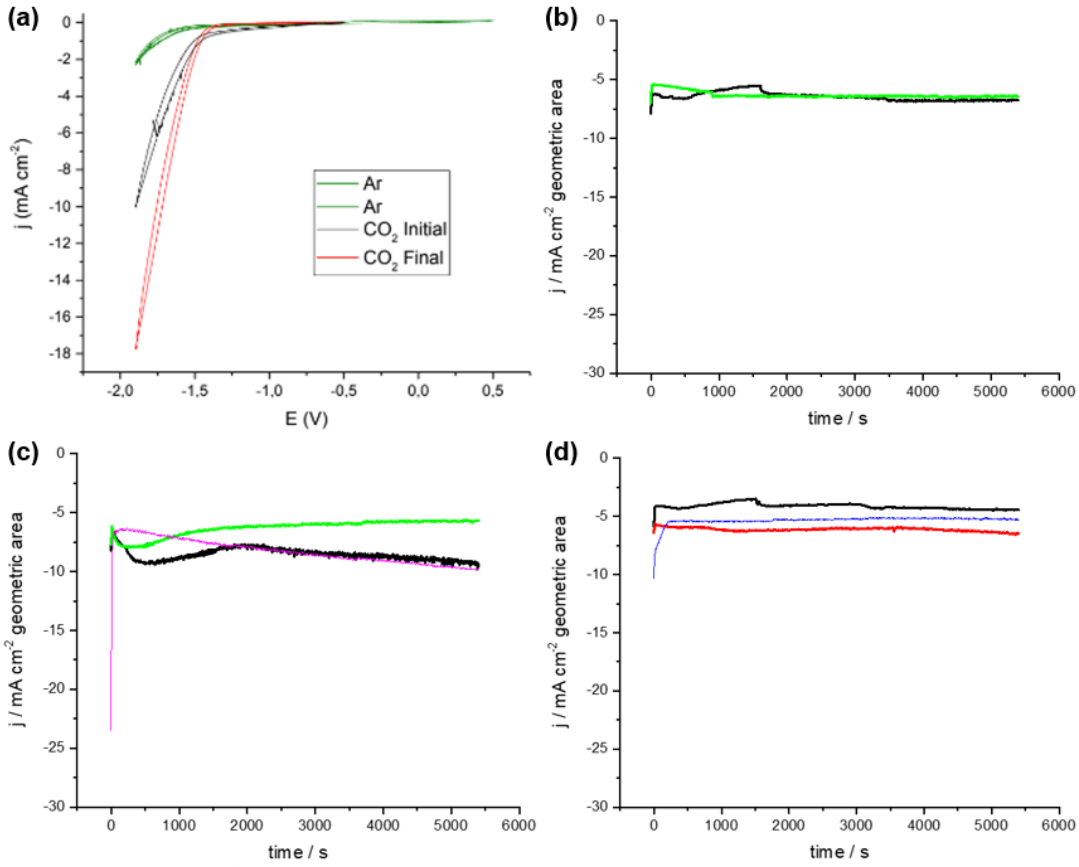

***Figure 12**. (a) Cyclic voltammetry of Bi400 with loading of 1 mg cm^{-2}, (b) Bi400 stability measurements at -1,7 V, (c) Bi500 stability measurements at -1,7 V, (d) Bi600 stability measurements at -1,7 V*

All the Faradaic efficiency values after 30 and 90 minutes can be seen in Table 1. The FE of the samples increased with the increase of carbonization temperature and reached 100% after 90 minutes in sample Bi600 and in sample Bi700, the FE decreased drastically. The potentiometric measurements for samples Bi400 – Bi600 can be seen in Figure 12b,c,d. Based on the data in Table 1, samples Bi300 and Bi700 were excluded from the potentiometric measurements since the FE values were too low. The current density values were similar to those reported in previous studies [35]. From the potentiometric measurements, we can see that sample Bi600 was more stable than the other two samples. While sample Bi600 has a FE of 100 % after 90 minutes, but early in the measurement, after 30 minutes, sample Bi600 shows FE up to 111%, which indicates that at the beginning of the measurement some side reactions took place in the cell, which stabilised by the

next measurement at 90 minutes. Other samples which were carbonized at lower temperatures or higher temperatures than 600 °C show significantly lower FE values and none of the seem to show obvious possibilities of side reactions. The fact that in sample Bi600, FE of 100 % was observed means that the contribution of HER is very minor and possibly even negligible, accounting for experimental error.

Table 1. *Electrochemical measurement results*

	Bi300	**Bi400**	**Bi500**	**Bi600**	**Bi700**
FE (%) – 0.5h	75-70	100-97	89-87	111-110	68-76
FE (%) – 1.5h	59-47	99-93	96-81	100-98	73-69

From these results, we can clearly assume that sample Bi600 has the higher affinity for CO_2RR and the reaction taking place has the highest efficiency of the measured samples.

Further stability tests were conducted with samples Bi400 – Bi600 to see how the samples acted after longer periods of time. Potentiometric measurements were conducted over 4 hours and the graph can be seen in Figure 13. The results of the measurements can be seen in Table 2.

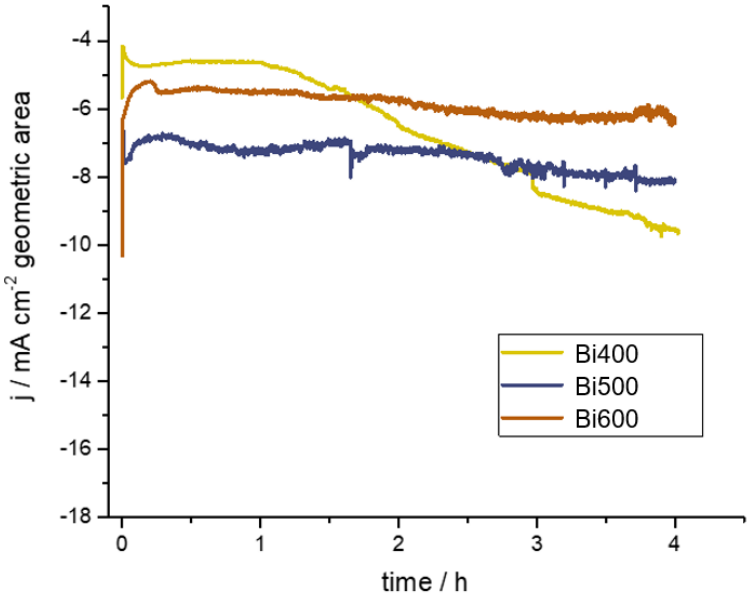

Figure 13*. Bi400, Bi500, Bi600 stability measurements at -1,7 V*

From the values in Table 2, we can clearly see that in sample Bi400, the FE decreased drastically after 4 hours of CO_2RR to formic acid. Sample Bi500 showed a less drastic decrease in FE and sample Bi600 only showed a decrease of 6 % after 4 hours, which is remarkably less than the other samples.

***Table 2**. Stability experiment results*

	Bi400	**Bi500**	**Bi600**
FE (%) – 0.5h	100-97	89-87	111-110
FE (%) – 1/2/3/4h	92/76/63/55	100/94/92/89	100/95/93/94

3.2.2 Morphology studies: XPS and XRD

To investigate the morphology of the catalysts and to understand why sample Bi600 was more electrochemically active and stable than the other samples, XRD and XPS analysis were conducted. XRD data confirms the presence of amorphous carbon material and bismuth in all carbonised samples. From the XRD data patterns in Figure 14a, we can see two sharp peaks at 38º and 40º which indicate, that bismuth present in metallic state with some features related to Bi oxides.

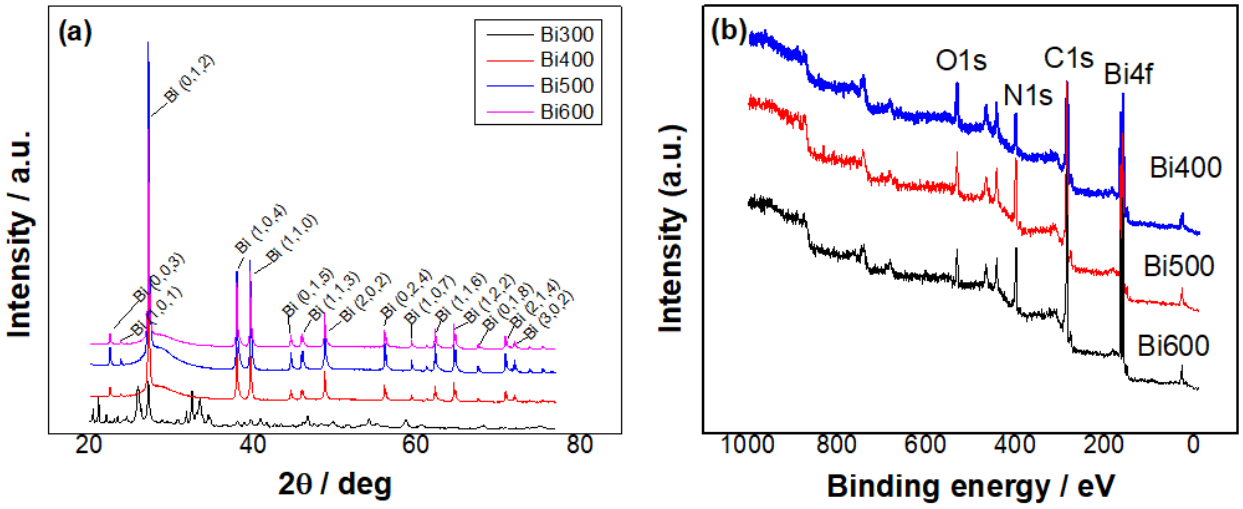

***Figure 14**. (a) XRD patterns, (b) XPS survey spectra*

To investigate the chemical composition and surface chemical state of the most active samples (Bi400, Bi500, Bi600), XPS measurements were carried out. As in Figure 14b, the survey spectra of the three samples show that all the materials consist of Bi, C, O and N elements and that their average concentrations are similar. Table 3 summarizes surface elemental composition of sample components. All materials do not contain other elements besides Bi, C, O and N in noticeable scale. The bismuth atomic concentration on the surface of catalyst materials is fairly equal, while the concentration of oxygen, carbon and nitrogen varies with samples. A trend can be seen with the oxygen concentrations, as the concentration decreases with increased carbonization temperature. While carbon and nitrogen atomic concentrations do not show any obvious trends.

Table 3.*Complete elemental content of the three main samples*

catalyst	Surface elemental composition (at.%)			
	Bi	C	N	O
Bi400	2.6	70.2	15.3	11.9
Bi500	2.3	67.9	20.3	9.6
Bi600	2.4	71.5	18.5	7.7

High-resolution spectra of Bi 4f peaks for the samples are given in Figure 15a, b, d. The peaks at binding energies 159 eV and 165 eV correspond to Bi $4f_{5/2}$ and Bi $4f_{7/2}$, which indicate that bismuth has an oxidation state of +3. Summarised fitting data in Table 4 indicates, that the bismuth particles in all samples have same oxidation state and that all three samples have fairly similar amounts of Bi particles, meaning that the increased activity does not come from higher amounts of Bi in the catalyst.

Table 4*. Relative content of of bismuth species in samples*

catalyst	Bi total (at.%)	Bi $4f_{7/2}$ (at.%)	Bi $4f_{5/2}$ (at.%)
Bi400	2.6	57.1	42.9
Bi500	2.3	57.4	42.6
Bi600	2.4	56.9	43.1

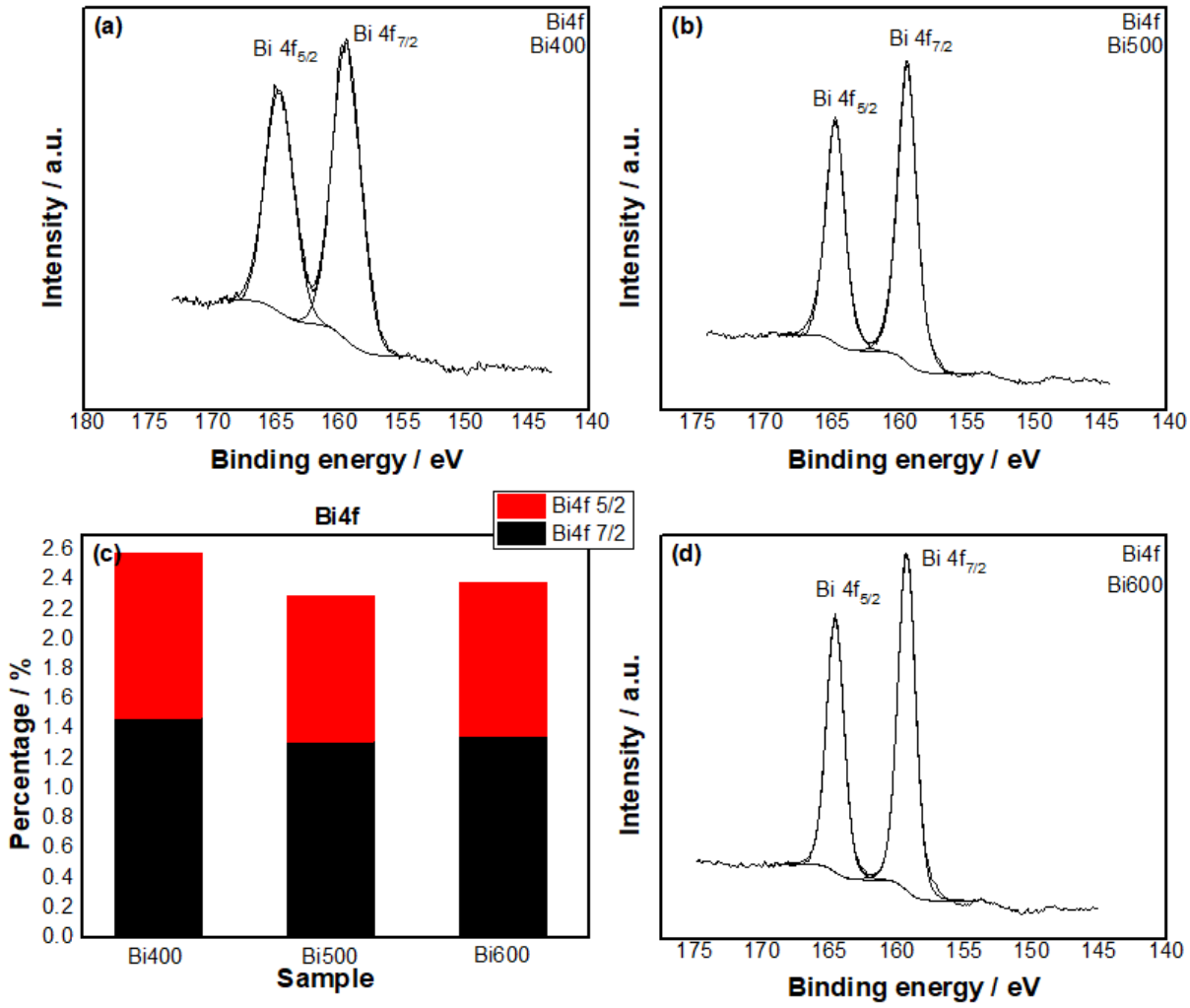

Figure 15. *High-resolution Bi 4f Spectra of (a) Bi400, (b) Bi500, and (d) Bi600 samples; (c) Bi 4f state composition histogram.*

Figure 16 represents high-resolution C 1s spectra of all three samples. C 1s spectra consists of the following peaks: sp^2, sp^3, carbide, C-O, C=O and π–π^*. These show the bonds found in the carbon backbone of the Bi-N-C material. It can be seen that the carbide peak is much larger in Bi400 than in the other samples, which means that in samples Bi500 and Bi600, the bismuth particles did not form as many bonds with the carbon backbone as sample Bi400 did. From Table 5 it can be seen, that besides Bi400 forming more carbon bonds, the three samples have similar amounts of different carbon compounds, which means that mostly the carbon backbone of the samples was similar.

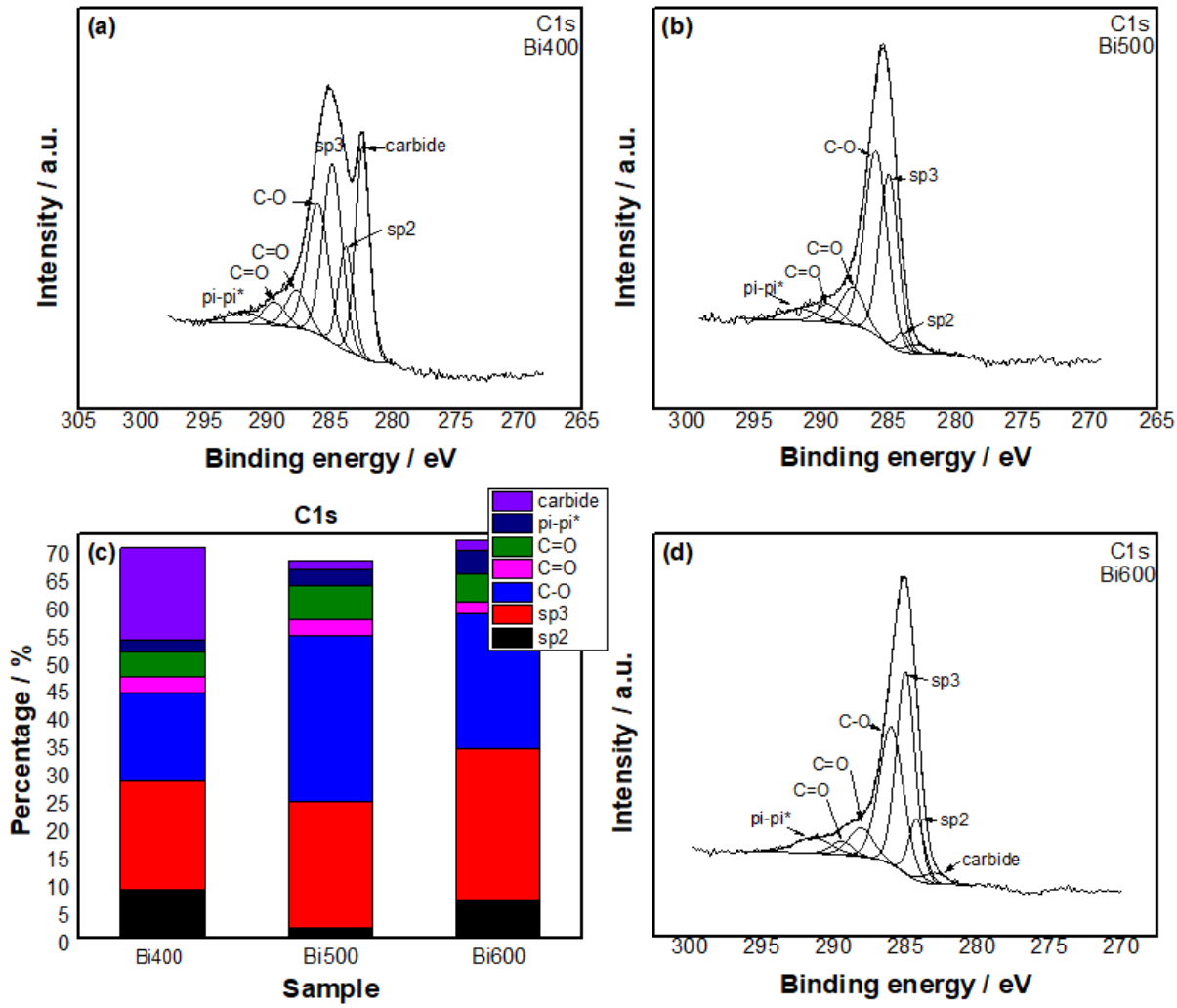

***Figure 16**. High-resolution C 1s spectra of (a) Bi400, (b) Bi500, and (d) Bi600 samples; (c) C 1s state composition histogram.*

***Table 5**. Relative content of carbon species in samples*

catalyst	C total (at%)	sp2 (%)	sp3 (%)	C-O (%)	C=O (%)	C=O (%)	pi-pi* (%)	carbide (%)
Bi400	70.2	12.2	28	22.5	4.1	6.5	29	23.8
Bi500	67.9	2.5	33.7	43.9	4.3	9.1	4.3	2.2
Bi600	71.5	9.7	38.1	33.9	3	7.1	5.7	2.5

Figure 17 shows the core-level XPS spectra in the N 1s region. The spectra consists of peaks corresponding to NO, bulk N-h, Graphitic-N, Pyrrolic-N, Imine, Pyridinic-N and Metal-N_x species. In sample Bi400, the metal-N_x peak was remarkably large and in sample Bi500, it was

also rather large, while in sample Bi600, it was quite a bit smaller than in both other samples. This indicates that in samples Bi400 and Bi500, the Bi particles form much more coordinate bonds with nitrogen compounds than in sample Bi600. Relative oncentrations of different nitrogen compounds found in the samples can be seen in Table 6.

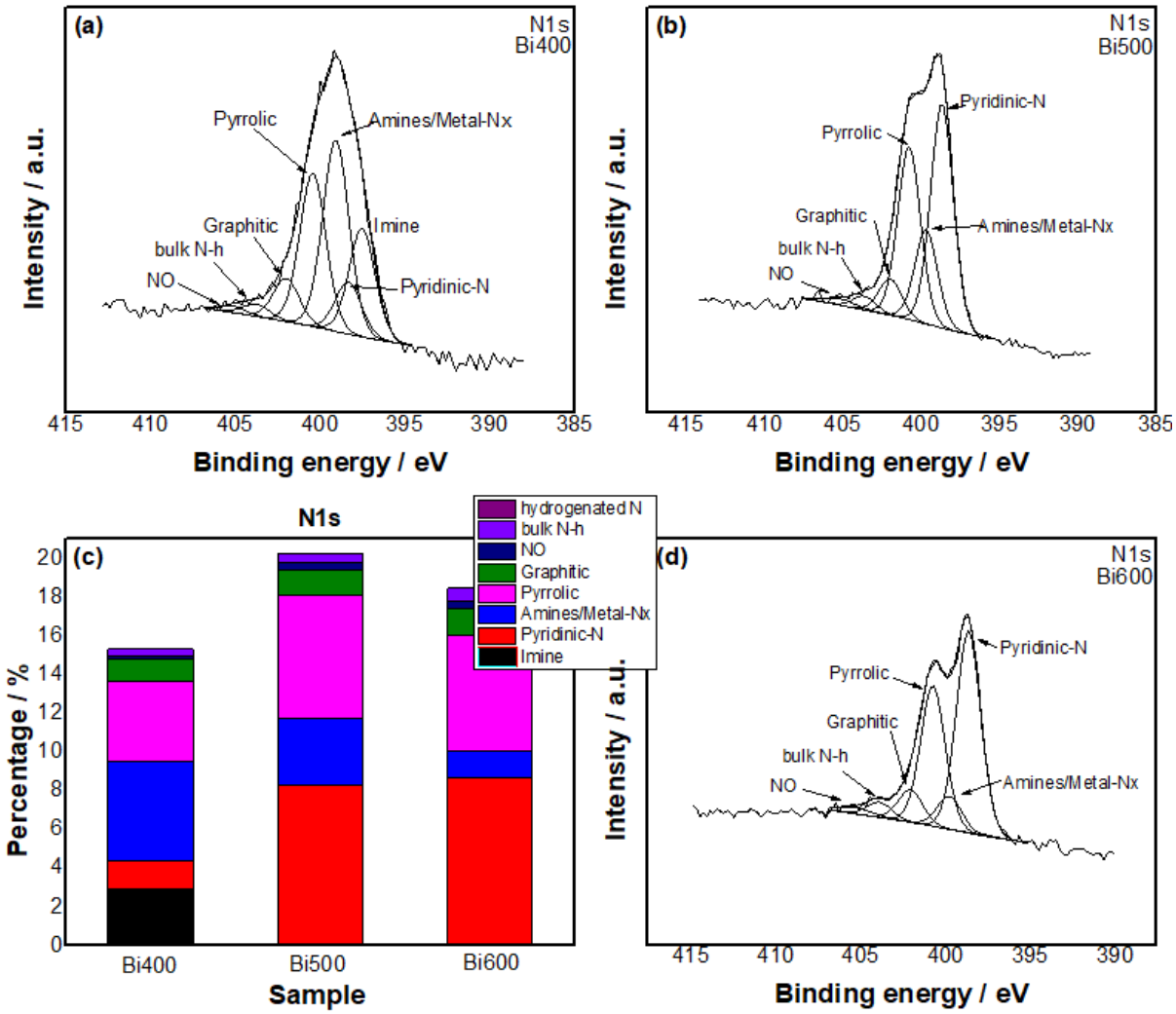

Figure 17*. High-resolution N 1s spectra of (a) Bi400, (b) Bi500, and (d) Bi600 samples; (c) N 1s state composition histogram.*

Table 6. *Relative content of nitrogen species in samples*

catalyst	N total (at%)	Imine (%)	Pyridinic-N (%)	Amines/Metal-NX (%)	Pyrrolic (%)	Graphitic (%)	NO (%)	Bulk N-h (%)
Bi400	15.3	19.1	9.2	33.7	27	7.6	1.2	2.2
Bi500	20.3	0	40.7	17	31.5	6.6	1.7	2.5
Bi600	18.5	0.3	46.6	7.6	32.5	7.5	2	3.5

Figure 18 shows core-level XPS spectra in the O 1s region. Fitted O 1s spectra consist of the following oxygen species: C-O, C-OH, water, C=O, metal oxide and O=C-OH. In samples Bi400 and Bi500, the metal oxide peak is larger than in sample Bi600. Summarized data in Table 7 indicates, that the samples have quite different ratios of different oxygen-containing compounds, but it can be clearly seen that at lower temperatures, more oxides form.

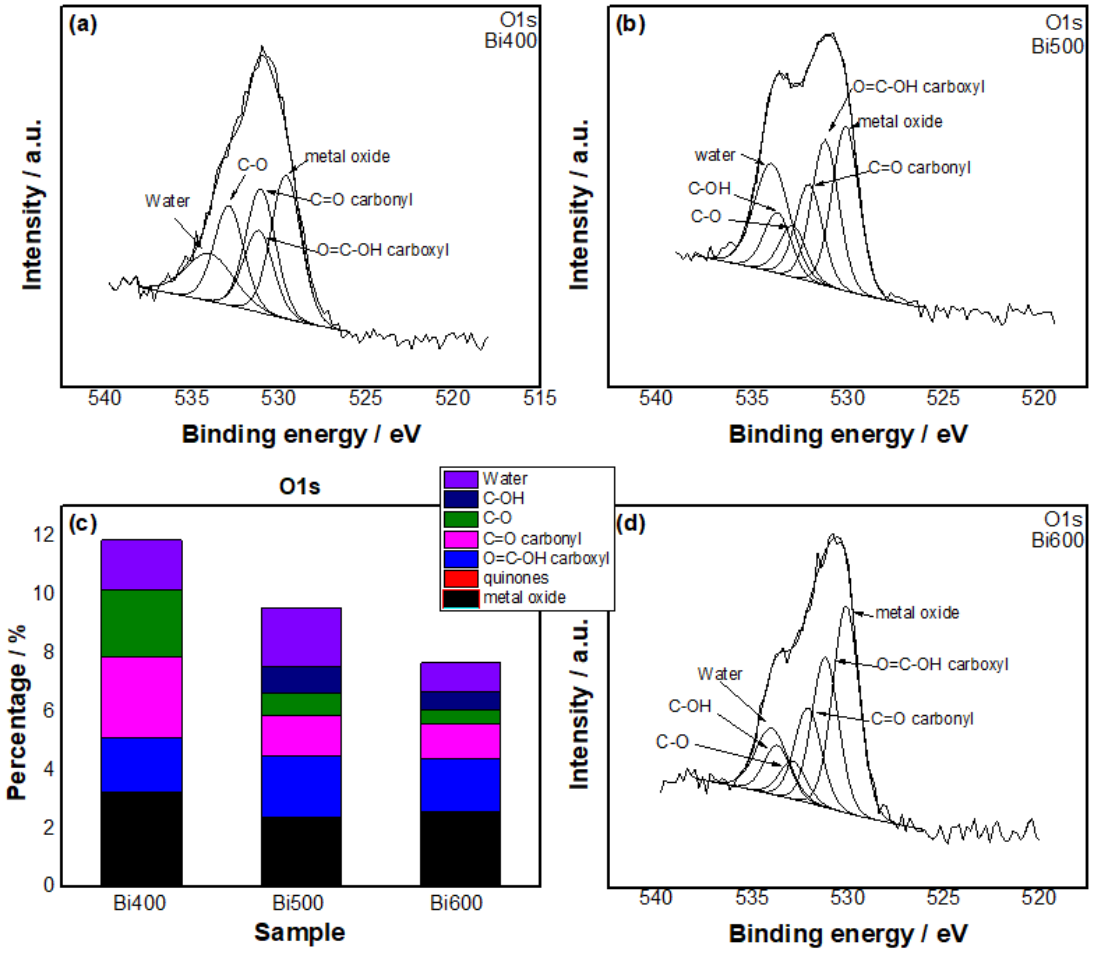

Figure 18. *High-resolution O 1s spectra of (a) Bi400, (b) Bi500, and (d) Bi600 samples; (c) O 1s state composition histogram.*

Table 7. *Relative content of oxygen species in samples*

catalyst	O total (at%)	Metal oxide (%)	O=C-OH carboxyl (%)	C=O carbonyl (%)	C-O (%)	C-OH (%)	Water (%)
Bi400	11.9	27.3	15.6	23.6	19	0	14.5
Bi500	9.2	24.9	22	14.7	7.8	9.2	21.4
Bi600	7.7	33.3	24.2	15.3	6.1	8.1	13

From the XPS data, it can be deduced that in sample Bi600, the Bi particles from the least carbide, oxide and nitrogen bonds out of the measured samples. According to the XPS and XRD values, no other compounds besides bismuth, oxygen, nitrogen and carbon are in the lattice. The fewer other bonds Bi particles form, the more bonds they form with other Bi particles. Leading to larger particles of metallic bismuth. Metallic bismuth state in the Bi-N-C lattice leads to a more efficient CO_2RR reaction, higher stability and higher FE of CO_2 electroreduction to formic acid.

3.2.3 Microscopic imaging: SEM and TEM

To further investigate the surface morphology of the materials, and to understand the difference in electrocatalytic behaviour, TEM and SEM analysis was conducted. TEM images in Figure 19a and 20c indicate, that there is no clear structures formed and after carbonisation at 400 ºC bismuth exists predominantly in amorphous form. As can be seen from the SEM images of sample Bi400, in (Figure 19b,d) the surface of the catalyst material is not homogeneous, some small spherical particles and larger aggregates are formed.

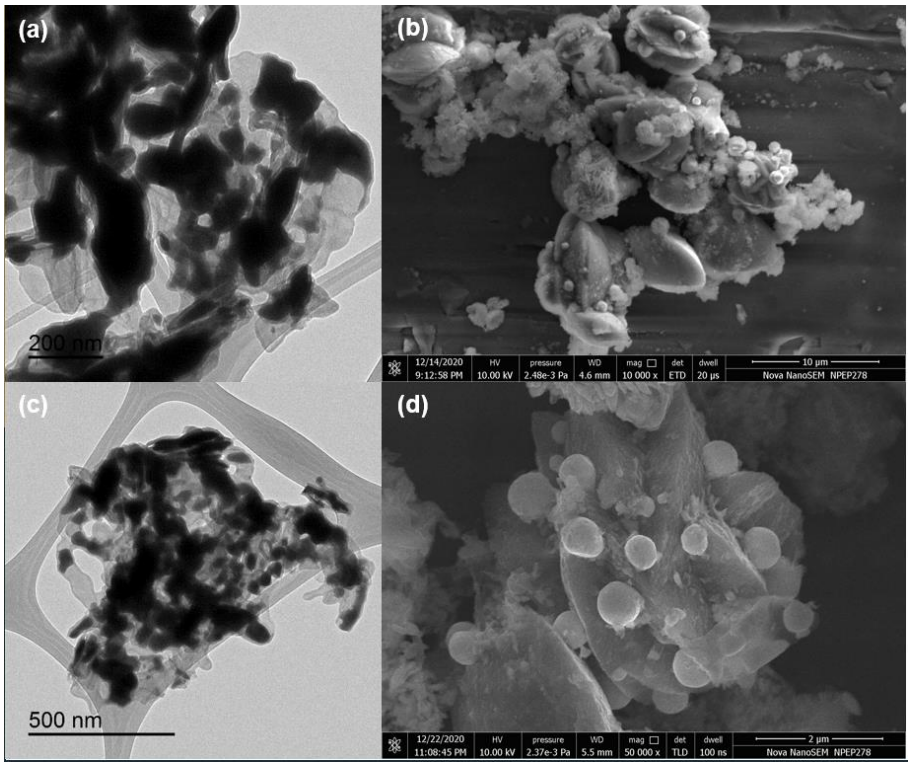

Figure 19*. (a,c) TEM and (b,d) SEM images of Bi400 sample*

As can be seen from Figure 20, there was no clear difference in sample morphology after carbonisation at 500 ºC. Some spherical particles can be seen on the surface of the material. In sample Bi500, the spherical particles are significantly bigger than in sample Bi400 (2 μm vs. 1 μm). In Figure 20a, the TEM images indicate the beginning of Bi nucleation and crystallization.

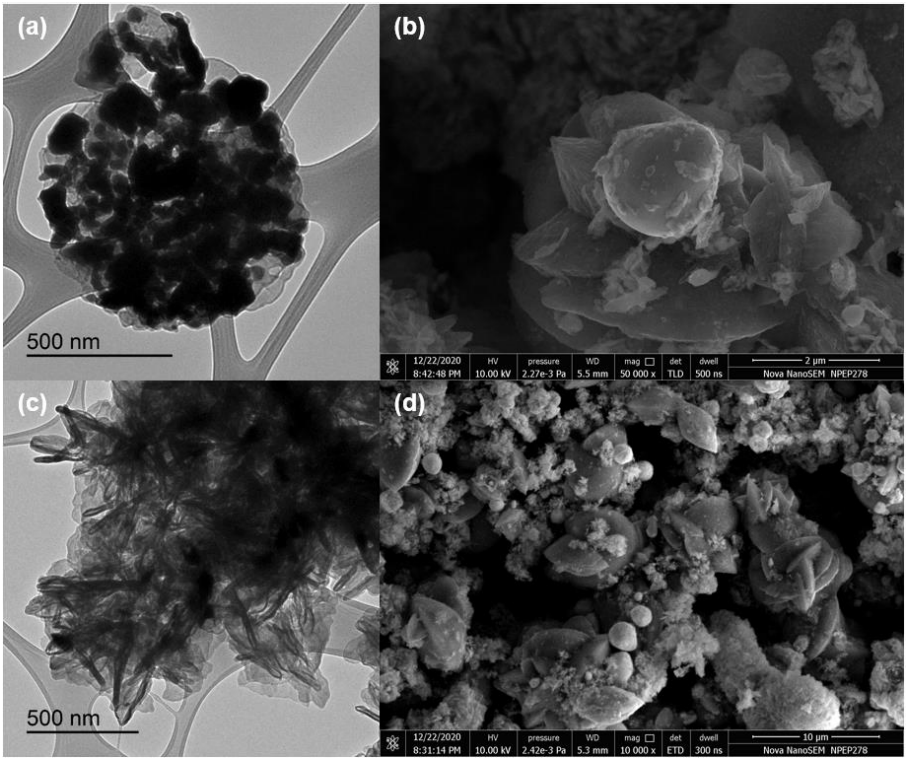

Figure 20. *(a,c) TEM and (b,d) SEM images of Bi500 sample*

Figure 21 clearly indicates that carbonisation of samples at 600 ºC result in formation of clearly crystallized structure of Bi metallic nanoparticles. In Figure 21a,c, the TEM images show clearly homogeneous distribution of spherical Bi nanoparticles with average size of 27±6 nm. As can be seen from SEM images in Figure 21b,d, Bi600 has non-homogeneous morphological structure.

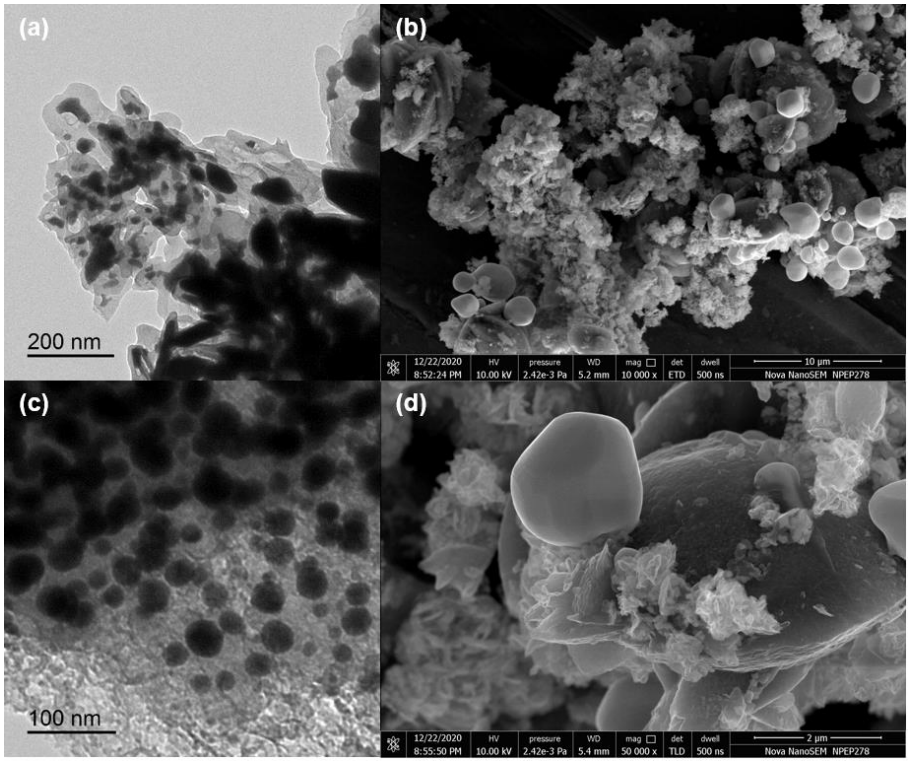

Figure 21. *(a,c) TEM and (b,d) SEM images of Bi500 sample*

The SEM and TEM analysis further prove the nucleation and formation of metallic Bi nanoparticles with increasing of carbonisation temperature. TEM analysis revealed the process of the transformation of bismuth from amorphous to crystalline phase.

3.2.4 DFT calculations

In order to confirm the positive effect of metallic Bi on CO_2 selective electroreduction to formic acid, we performed density functional theory (DFT) calculations (Figure 22). According to our preliminary calculations Bi (111) does show to be better catalyst for HCOOH formation with lower required potential than CO formation on Bi-N_4, so overall we can say that Bi600 is HCOOH selective. From Figure 22 we can say that speaking about Bi(111), the overpotential for formation

of HCOOH is 0.37 eV, while for formation of CO it is 0.996 eV; additionally if we consider BiN_4 the overpotential for formation of HCOOH is 1.056 eV and for formation of CO it is 0.553 eV.

As such overall the least overpotential is for HCOOH formation on Bi(111) surface, which is what we experimentally observe.

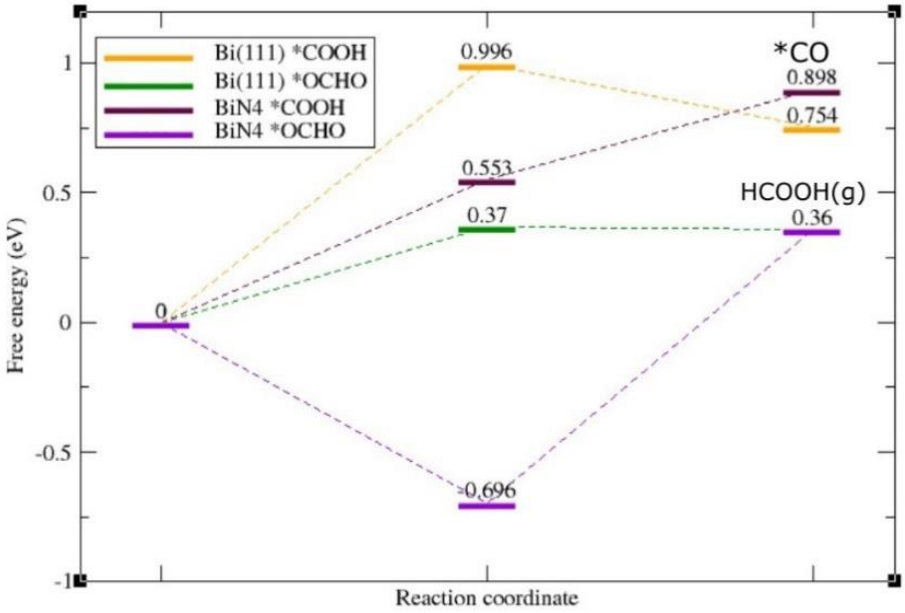

Figure 22. *Free energy diagram for CO and HCOOH formation on prepared Bi-C-N*

SUMMARY

In this work, Bi-N-C electrocatalysts were fabricated by optimised carbonization of TAL33 MOF material. Prepared catalysts exhibited promising results in CO_2RR to formic acid.

The structure, composition and morphology of the bismuth MOF based materials were analysed with scanning electron microscopy, transmission electron spectroscopy, X-ray diffraction and X-ray photoelectron spectroscopy. The electrocatalytic activity and stability of the bismuth MOF based catalysts towards CO_2 electroreduction was investigated in $KHCO_3$ solution using cycling voltammetry and potentiometric measurements.

Overall, five different samples were studied (carbonization temperatures 300-700 °C) and obtained FE values varied between 47 – 100 % after 90 minutes of testing. Carbonisation of sample at 600 °C resulted in the highest efficiency as well as highest stability in time, with the loss of only 6 % of FE after 4 hours of stability testing. With sample Bi600 reaching FE of 100 %, HER plays a negligible role in the reaction, meaning that only CO_2RR takes place in the cell. According to surface morphological investigations, sample Bi600 showed higher activity than the rest of the samples because the bismuth particles in Bi600 formed more metallic bismuth bonds. SEM and TEM measurements indicated the process of the transformation of bismuth from amorphous to crystalline phase. Results were further confirmed by DFT calculations.

ACKNOWLEDGEMENTS

I would like to thank my amazing supervisor Dr. Nadezda Kongi for all her guidance and support throughout the project.

I would like to thank Dr. Jaan Aaruväli (UT) for the XRD measurements, Dr. Sergei Vlassov (UT) for the SEM images, Dr. Arvo Kikas and Dr. Vambola Kisand (UT) for the XPS measurements, and Dr. Pavel Starkov (TalTech) for the TAL33 starting material. Special thanks to Beatriz Ávila-Bolívar and Prof. José Solla-Gullón (University of Alicante, Spain) for the TEM images and electrochemical measurements. Big thanks to Ritums Cepitis (UT) for DFT calculations. This work was supported by the Estonian Research Council grant (PSG250).

REFERENCES

(1) Apadula, F.; Cassardo, C.; Ferrarese, S.; Heltai, D.; Lanza, A. Thirty Years of Atmospheric CO2 Observations at the Plateau Rosa Station, Italy. *Atmosphere* **2019**, *10* (7), 418. https://doi.org/10.3390/atmos10070418.

(2) Albo, J.; Alvarez-Guerra, M.; Castaño, P.; Irabien, A. Towards the Electrochemical Conversion of Carbon Dioxide into Methanol. *Green Chem.* **2015**, 21.

(3) CO2 Electroreduction to Formate_ Continuous Single-Pass Operation in a Filter-Press Reactor at High Current Densities Using Bi Gas Diffusion Electrodes. **2019**, 8.

(4) Ma, J.; Sun, N.; Zhang, X.; Zhao, N.; Xiao, F.; Wei, W.; Sun, Y. A Short Review of Catalysis for CO2 Conversion. *Catal. Today* **2009**, *148* (3–4), 221–231. https://doi.org/10.1016/j.cattod.2009.08.015.

(5) Qiao, J.; Liu, Y.; Hong, F.; Zhang, J. A Review of Catalysts for the Electroreduction of Carbon Dioxide to Produce Low-Carbon Fuels. *Chem Soc Rev* **2014**, *43* (2), 631–675. https://doi.org/10.1039/C3CS60323G.

(6) Zhang, R.-Z.; Wu, B.-Y.; Li, Q.; Lu, L.-L.; Shi, W.; Cheng, P. Design Strategies and Mechanism Studies of CO2 Electroreduction Catalysts Based on Coordination Chemistry. *Coord. Chem. Rev.* **2020**, *422*, 213436. https://doi.org/10.1016/j.ccr.2020.213436.

(7) Kang, P.; Chen, Z.; Brookhart, M.; Meyer, T. J. Electrocatalytic Reduction of Carbon Dioxide: Let the Molecules Do the Work. *Top. Catal.* **2015**, *58* (1), 30–45. https://doi.org/10.1007/s11244-014-0344-y.

(8) *Electrochemical Reduction of Carbon Dioxide: Fundamentals and Technologies*; Qiao, J., Liu, Y., Zhang, J., Eds.; Electrochemical Energy Storage and Conversion; CRC Press, 2016. https://doi.org/10.1201/b20177.

(9) Hori, Y. Electrochemical CO2 Reduction on Metal Electrodes. In *Modern Aspects of Electrochemistry*; Vayenas, C. G., White, R. E., Gamboa-Aldeco, M. E., Eds.; Modern Aspects of Electrochemistry; Springer New York: New York, NY, 2008; Vol. 42, pp 89–189. https://doi.org/10.1007/978-0-387-49489-0_3.

(10) Sun, Z.; Ma, T.; Tao, H.; Fan, Q.; Han, B. Fundamentals and Challenges of Electrochemical CO2 Reduction Using Two-Dimensional Materials. *Chem* **2017**, *3* (4), 560–587. https://doi.org/10.1016/j.chempr.2017.09.009.

(11) Finn, C.; Schnittger, S.; Yellowlees, L. J.; Love, J. B. Molecular Approaches to the Electrochemical Reduction of Carbon Dioxide. *Chem Commun* **2012**, *48* (10), 1392–1399. https://doi.org/10.1039/C1CC15393E.

(12) Zhu, D. D.; Liu, J. L.; Qiao, S. Z. Recent Advances in Inorganic Heterogeneous Electrocatalysts for Reduction of Carbon Dioxide. *Adv. Mater.* **2016**, *28* (18), 3423–3452. https://doi.org/10.1002/adma.201504766.

(13) Shan, C.; Martin, E. T.; Peters, D. G.; Zaleski, J. M. Site-Selective Growth of AgPd Nanodendrite-Modified Au Nanoprisms: High Electrocatalytic Performance for CO_2 Reduction. *Chem. Mater.* **2017**, *29* (14), 6030–6043. https://doi.org/10.1021/acs.chemmater.7b01813.

(14) Lee, C. W.; Cho, N. H.; Nam, K. T.; Hwang, Y. J.; Min, B. K. Cyclic Two-Step Electrolysis for Stable Electrochemical Conversion of Carbon Dioxide to Formate. *Nat. Commun.* **2019**, *10* (1), 3919. https://doi.org/10.1038/s41467-019-11903-5.

(15) Loges, B.; Boddien, A.; Gärtner, F.; Junge, H.; Beller, M. Catalytic Generation of Hydrogen from Formic Acid and Its Derivatives: Useful Hydrogen Storage Materials. *Top. Catal.* **2010**, *53* (13–14), 902–914. https://doi.org/10.1007/s11244-010-9522-8.

(16) Alfath, M.; Lee, C. W. Recent Advances in the Catalyst Design and Mass Transport Control for the Electrochemical Reduction of Carbon Dioxide to Formate. *Catalysts* **2020**, *10* (8), 859. https://doi.org/10.3390/catal10080859.

(17) Rumayor, M.; Dominguez-Ramos, A.; Perez, P.; Irabien, A. A Techno-Economic Evaluation Approach to the Electrochemical Reduction of CO2 for Formic Acid Manufacture. *J. CO2 Util.* **2019**, *34*, 490–499. https://doi.org/10.1016/j.jcou.2019.07.024.

(18) Global Formic Acid Market Report, History and Forecast 2020-2027. *Dataintelo*.

(19) Kortlever, R.; Shen, J.; Schouten, K. J. P.; Calle-Vallejo, F.; Koper, M. T. M. Catalysts and Reaction Pathways for the Electrochemical Reduction of Carbon Dioxide. *J. Phys. Chem. Lett.* **2015**, *6* (20), 4073–4082. https://doi.org/10.1021/acs.jpclett.5b01559.

(20) Komatsu, S.; Tanaka, M.; Okumura, A.; Kungi, A. Preparation of Cu-Solid Polymer Electrolyte Composite Electrodes and Application to Gas-Phase Electrochemical Reduction of CO2. *Electrochimica Acta* **1995**, *40* (6), 745–753. https://doi.org/10.1016/0013-4686(94)00325-U.

(21) Sreekanth, N.; Phani, K. L. Selective Reduction of CO_2 to Formate through Bicarbonate Reduction on Metal Electrodes: New Insights Gained from SG/TC Mode of SECM. *Chem Commun* **2014**, *50* (76), 11143–11146. https://doi.org/10.1039/C4CC03099K.

(22) Deng, P.; Wang, H.; Qi, R.; Zhu, J.; Chen, S.; Yang, F.; Zhou, L.; Qi, K.; Liu, H.; Xia, B. Y. Bismuth Oxides with Enhanced Bismuth–Oxygen Structure for Efficient Electrochemical Reduction of Carbon Dioxide to Formate. *ACS Catal.* **2020**, *10* (1), 743–750. https://doi.org/10.1021/acscatal.9b04043.

(23) Bertin, E.; Garbarino, S.; Roy, C.; Kazemi, S.; Guay, D. Selective Electroreduction of CO 2 to Formate on Bi and Oxide-Derived Bi Films. *J. CO2 Util.* **2017**, *19*, 276–283. https://doi.org/10.1016/j.jcou.2017.04.006.

(24) Koh, J. H.; Won, D. H.; Eom, T.; Kim, N.-K.; Jung, K. D.; Kim, H.; Hwang, Y. J.; Min, B. K. Facile CO_2 Electro-Reduction to Formate via Oxygen Bidentate Intermediate Stabilized by High-Index Planes of Bi Dendrite Catalyst. *ACS Catal.* **2017**, *7* (8), 5071–5077. https://doi.org/10.1021/acscatal.7b00707.

(25) School of Chemistry and Chemical Engineering, Jiangsu University, Zhenjiang 212013, P. R. China; Shao, L. A Highly Efficient Bi-Based Electrocatalyst for the Reduction of CO2 to Formate. *Int. J. Electrochem. Sci.* **2019**, 114–125. https://doi.org/10.20964/2019.01.28.

(26) Lee, C. W.; Hong, J. S.; Yang, K. D.; Jin, K.; Lee, J. H.; Ahn, H.-Y.; Seo, H.; Sung, N.-E.; Nam, K. T. Selective Electrochemical Production of Formate from Carbon Dioxide with Bismuth-Based Catalysts in an Aqueous Electrolyte. *ACS Catal.* **2018**, *8* (2), 931–937. https://doi.org/10.1021/acscatal.7b03242.

(27) Su, P.; Xu, W.; Qiu, Y.; Zhang, T.; Li, X.; Zhang, H. Ultrathin Bismuth Nanosheets as a Highly Efficient CO_2 Reduction Electrocatalyst. *ChemSusChem* **2018**, *11* (5), 848–853. https://doi.org/10.1002/cssc.201702229.

(28) Zhong, H.; Qiu, Y.; Zhang, T.; Li, X.; Zhang, H.; Chen, X. Bismuth Nanodendrites as a High Performance Electrocatalyst for Selective Conversion of CO_2 to Formate. *J. Mater. Chem. A* **2016**, *4* (36), 13746–13753. https://doi.org/10.1039/C6TA06202D.

(29) Wain, A. J. Scanning Electrochemical Microscopy for Combinatorial Screening Applications: A Mini-Review. *Electrochem. Commun.* **2014**, *46*, 9–12. https://doi.org/10.1016/j.elecom.2014.05.028.

(30) Ge, M.; Wang, Y.; Carraro, F.; Liang, W.; Roostaeinia, M.; Siahrostami, S.; Proserpio, D. M.; Doonan, C.; Falcaro, P.; Zheng, H.; Zou, X.; Huang, Z. High-Throughput Electron Diffraction Reveals a Hidden Novel Metal–Organic Framework for Electrocatalysis. *Angew. Chem. Int. Ed.* **2021**, *60* (20), 11391–11397. https://doi.org/10.1002/anie.202016882.

(31) Zhang, B.; Cao, S.; Wu, Y.; Zhai, P.; Li, Z.; Zhang, Y.; Fan, Z.; Wang, C.; Zhang, X.; Hou, J.; Sun, L. Metal-Organic-Framework-Derived Bismuth Nanosheets for Electrochemical and Solar-Driven Electrochemical CO_2 Reduction to Formate. *ChemElectroChem* **2021**, *8* (5), 880–886. https://doi.org/10.1002/celc.202001613.

(32) Cao, C.; Ma, D.; Gu, J.; Xie, X.; Zeng, G.; Li, X.; Han, S.; Zhu, Q.; Wu, X.; Xu, Q. Metal–Organic Layers Leading to Atomically Thin Bismuthene for Efficient Carbon Dioxide Electroreduction to Liquid Fuel. *Angew. Chem. Int. Ed.* **2020**, *59* (35), 15014–15020. https://doi.org/10.1002/anie.202005577.

(33) Yuan, W.-W.; Wu, J.-X.; Zhang, X.-D.; Hou, S.-Z.; Xu, M.; Gu, Z.-Y. *In Situ* Transformation of Bismuth Metal–Organic Frameworks for Efficient Selective Electroreduction of CO_2 to Formate. *J. Mater. Chem. A* **2020**, *8* (46), 24486–24492. https://doi.org/10.1039/D0TA08092F.

(34) Ping, K.; Alam, M.; Käärik, M.; Leis, J.; Kongi, N.; Järving, I.; Starkov, P. Surveying Iron–Organic Framework TAL-1-Derived Materials in Ligandless Heterogeneous Oxidative Catalytic Transformations of Alkylarenes. *Synlett* **2019**, *30* (13), 1536–1540. https://doi.org/10.1055/s-0037-1611877.

(35) Ávila-Bolívar, B.; García-Cruz, L.; Montiel, V.; Solla-Gullón, J. Electrochemical Reduction of CO2 to Formate on Easily Prepared Carbon-Supported Bi Nanoparticles. *Molecules* **2019**, *24* (11), 2032. https://doi.org/10.3390/molecules24112032.

NON-EXCLUSIVE LICENCE TO REPRODUCE THESIS AND MAKE THESIS PUBLIC

I, Jürgen-Martin Assafrei

1. herewith grant the University of Tartu a free permit (non-exclusive licence) to reproduce, for the purpose of preservation, including for adding to the DSpace digital archives until the expiry of the term of copyright,

"Bismuth Metal-Organic Framework Based Catalyst for CO_2 Electroreduction" supervised by Assoc. Prof. Nadezda Kongi.

2. I grant the University of Tartu a permit to make the work specified in p. 1 available to the public from ***20/05/2026*** via the web environment of the University of Tartu, including via the DSpace digital archives, under the Creative Commons licence CC BY NC ND 3.0, which allows, by giving appropriate credit to the author, to reproduce, distribute the work and communicate it to the public, and prohibits the creation of derivative works and any commercial use of the work until the expiry of the term of copyright.

3. I am aware of the fact that the author retains the rights specified in p. 1 and 2.

4. I certify that granting the non-exclusive licence does not infringe other persons' intellectual property rights or rights arising from the personal data protection legislation.

Jürgen-Martin Assafrei

20/05/2021